ATLAS Internal Note
PHYS-No-111
October 1997

Precision SUSY measurements with ATLAS for SUGRA point 5

Giacomo Polesello
INFN, Sezione di Pavia, Via Bassi 6, Pavia, Italy

Luc Poggioli
CERN, PPE Division, 1211 Geneva 23 Switzerland

Elżbieta Richter-Wąs [1]
Institute of Computer Science, Jagellonian University,
Institute of Nuclear Physics
30-059 Krakow, ul.Kawiory 26a, Poland

Jesper Söderqvist
Royal Institute of Technology (KTH), Stockholm, Sweden

Abstract

In the framework of the SUSY simulation studies in the ATLAS Collaboration, 5 sample points in SUGRA parameter space were studied. This paper presents studies on exclusive signatures for events produced at the point defined by the SUGRA parameters: $m_0 = 100$ GeV; $m_{1/2} = 300$ GeV; A = 300 GeV; tan$\beta = 2.1$; $\mu > 0$ (conventionally Point 5). It is shown that in this point the masses of squarks and sleptons can be measured, allowing to put significant constraints on the fundamental parameters of the theory

[1]Supported in part by Polish Government funds 2P03B00212 and 2P03B17210

1 Introduction

The work performed for the ATLAS Technical Proposal [1], as well as many other phenomenological studies [2], have shown that, if the scale of squark and gluino masses is below $\approx$ 2 TeV and R–Parity is conserved, SUSY will easily be discovered at the LHC, by employing inclusive signatures including E_T^{miss} and jets and/or leptons. However, such inclusive signatures, explicitly aimed at covering the broadest possible range of SUSY models, will give little information about the underlying model.

If SUSY is discovered at the LHC, a fundamental challenge for LHC experiments will be to constrain the model describing the observed signatures, and to measure its free parameters.
The Minimal Supersymmetric Standard Model (MSSM) on which the Technical Proposal studies were based, is very general, and has a large number of free parameters, notably all the sfermion masses. It is therefore impossible in the MSSM to combine the information from the different experimentally accessible final states to constrain the fundamental parameters of the model.

In order to overcome this problem, the ATLAS collaboration chose to study a relatively well–constrained model (SUGRA)[2]. Detailed studies have been performed on 5 sample points to verify the feasibility of model parameter extraction. The results have been presented to the LHCC, and the transparencies are available as [3].

A series of notes giving detailed information on the analyses performed on the 5 sample points have been written [4]–[8]. This note concentrates on point 5, defined by the following SUGRA parameters.:

m_0 = 100 GeV; $m_{1/2}$= 300 GeV; A = 300 GeV; tanβ= 2.1; $\mu > 0$.

2 Event generators and detector simulation

Only very short descriptions of the technical details of the simulation will be given here, as they can already be found in the accompanying notes [4]–[7].

2.1 Event generators

Two Monte Carlo generators for SUGRA are available, ISAJET [9] and SPYTHIA [10]. Both generators are in a status of rather fast evolution, and the following

considerations are based on the versions SPYTHIA 2.08 and ISAJET 7.22, which were used for the studies presented here.

The main differences in the SUSY part of the two generators are:

- ISAJET includes a full SUGRA evolution package, whereas SPYTHIA only incorporates an approximate solution to the Renormalization Group Equations;
- the SUSY Higgs boson masses and couplings are calculated only to 1 loop in ISAJET, whereas the full 2-loop calculation of [11] is included in SPYTHIA.

Such differences may give, when studying exclusive signatures, quite different phenomenologies. Therefore, both generators have been modified for the studies presented here, so that both have the same input physical contents.

Extensive checks, described elsewhere [4], have been performed on the mass spectra and branching ratios for all the five points, to verify the consistency of the two generators. The results are quite satisfactory, except for the third generation sector, where some discrepancies still exist.

2.2 The Detector Simulation

The detector has been simulated with the ATLFAST package [12]. We refer the reader to the documentation of the package for details about the way the different relevant detector parameters are incorporated in the simulation.
The output of ATLFAST is then submitted to further treatment to simulate e.g. the b–tagging efficiency of the ATLAS detector and to re-calibrate the b–jet energies according to the algorithm described in [12]. We refer to [5] for a detailed discussion of the prescriptions introduced in the simulation.

2.3 Evaluation of parameters

The aim of the analyses presented in this note is the measurement of physical observables such as the masses and the couplings of the supersymmetric particles. The work usually proceeds through the identification of an exclusive channel which can be separated both from the Standard Model background and from other SUSY channels through appropriate cuts on the final state jets and leptons.
Once a clean sample of events is obtained, we build kinematic distributions which

should only be sensitive to the masses of the involved particles, and not to the details of the kinematics of the production of the primary SUSY particles. The basic problem is that in every event the two stable Lightest Supersymmetric Particles (LSP) escape detection, thus preventing the complete kinematical reconstruction.
Therefore a statistical procedure is adopted in most cases to evaluate the level of sensitivity of a given distribution to the masses of the participating particles.
The kinematical distributions are reproduced for a SUSY model where all parameters are kept fixed except for the mass of the particle under study, which is varied by a given amount.
The statistical 'distance' between the 'reference' and the variated distribution is then evaluated using a Kolmogorov–Smirnov test.

The dominant source of experimental systematic uncertainty considered here is the uncertainty on the mass scale of the ATLAS detector, which is estimated to be 0.1 % for electrons and muons and 1 % for hadronic jets

3 Characteristics of point 5

It is interesting, in the SUGRA parameter space, to map the region which is favoured by cosmological considerations [13] [14].

The argument is related to the possibility that a part of the Dark Matter in the universe is made up of the 'relic' neutralino density from the very early universe. The requirement of a relic neutralino density consistent with theoretical prejudices and astrophysical observations, puts constraints on the rate of annihilation of the lightest neutralinos. The rate depends on the masses of the virtual sparticles which are exchanged in the annihilation. In particular, the main annihilation channel for neutralinos in most of the parameter space is t–channel exchange of sleptons, which are therefore required to be relatively light, in order to provide the required annihilation rate.
Such constraints can be mapped onto the SUGRA parameter space, as shown in Fig. 1. The cosmologically favoured region is shown as contours of constant Ωh^2 in the (m_0, $m_{1/2}$) plane. Models with $0.025 \leq \Omega h^2 \leq 1$ are considered cosmologically interesting. Stricter bounds are imposed by assuming a specific cosmological scenario. A dominantly Cold Dark Matter inflationary universe would lie in between the $\Omega h^2 = 0.25$ and 0.75 contours. The COBE favoured MDM inflationary universe would lie between $\Omega h^2 = 0.15$ and 0.4 contours [14].
The point discussed in this note has been chosen in moderate slepton mass region favoured by cosmology. It will indeed be seen in the following that this requirement gives rise to a very distinctive phenomenology.

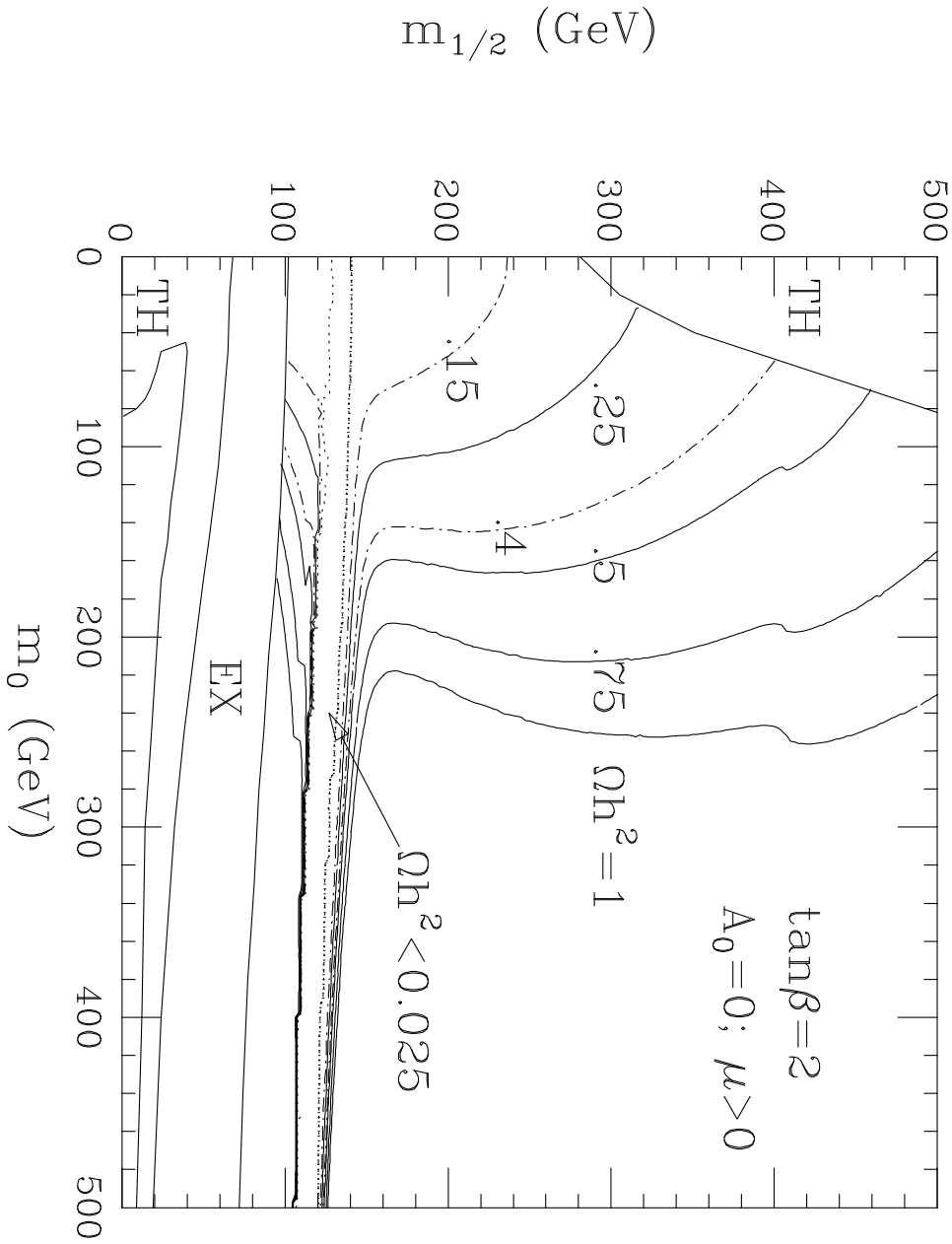

Figure 1: *Plots of contours of constant* Ωh^2 *in the* (m_0, $m_{1/2}$) *plane, where A=0,* $\mu > 0$, *and tanβ=2, and* $m_t = 170$ *GeV. The regions labelled by TH (EX) are excluded by theoretical (experimental) considerations. The pairs of contours 0.025–1, 0.25–0.75, 0.15–0.4 limit the regions favoured by different cosmological scenarios. (from [14])*

The main sparticle masses are shown in table 1:

Table 1: *Particle masses at point 5*

$m_{\tilde{q}_L} = 690$ GeV	$m_{\tilde{g}} = 770$ GeV
$m_{\tilde{q}_R} = 660$ GeV	$m_{\tilde{b}_1} = 630$ GeV
$m_{\tilde{t}_1} = 490$ GeV	$m_{\tilde{t}_2} = 710$ GeV
$m_{\tilde{\ell}_R} = 157$ GeV	$m_{\tilde{\ell}_L} = 240$ GeV
$m_{\tilde{\chi}_1^0} = 121$ GeV	$m_{\tilde{\chi}_2^0} = 232$ GeV
$m_h = 93$ GeV	$m_H = 640$ GeV

the lightest Higgs boson h is for this point at the limit of the region which will be explored by LEP 2. Squarks and gluinos are in the middle of the range accessible to LHC experimentation, and, as observed above, sleptons are relatively light.

The branching ratios relevant to studies which can be performed at the LHC are shown in Table 2.

Table 2: *Dominant branching ratios at point 5*

Decay			BR
$\tilde{g}$	$\rightarrow$	$\tilde{q}q$	65 %
		$\tilde{b}b$	25 %
		$\tilde{t}_1 t$	15 %
$\tilde{q}_L$	$\rightarrow$	$\tilde{\chi}_2^0 q$	33 %
		$\tilde{\chi}_1^+ q'$	65 %
$\tilde{q}_R$	$\rightarrow$	$\tilde{\chi}_1^0 q$	100 %
$\tilde{t}_1$	$\rightarrow$	$\tilde{\chi}_1^0 t$	70 %
		$\tilde{\chi}_2^0 t$	9 %
		$\tilde{\chi}_1^+ b$	21 %
$\tilde{\chi}_2^0$	$\rightarrow$	$\tilde{\chi}_1^0 h$	68 %
		$\tilde{\ell}_R l$	27 %
$\tilde{\chi}_1^\pm$	$\rightarrow$	$\tilde{\chi}_1^0 W$	98 %
$\tilde{\ell}$	$\rightarrow$	$\tilde{\chi}_1^0 l$	100 %
h	$\rightarrow$	bb	88 %

The total SUSY production cross–sections at point 5 is ≈ 19 pb. The different relevant contributions are given in Table 3. They are dominated by $\tilde{q}$ and $\tilde{g}$ strong production. Direct production of charginos and neutralinos, as well as

Table 3: *Production cross–sections for point 5*

Process	X-section (fb)
$pp \to \tilde{g}\tilde{g}$	1900
$pp \to \tilde{q}_L\tilde{q}_L$	1500
$pp \to \tilde{q}_R\tilde{q}_R$	1500
$pp \to \tilde{q}_L\tilde{q}_R$	2300
$pp \to \tilde{q}_L\tilde{g}$	4100
$pp \to \tilde{q}_R\tilde{g}$	4100
$pp \to \tilde{t}_1\tilde{t}_1$	680
$pp \to \tilde{\ell}\tilde{\ell}$ (l = e,μ)	65
$pp \to \tilde{\chi}_2^0\tilde{\chi}_1^\pm$	420
$pp \to \tilde{\chi}_1^\pm\tilde{\chi}_1^\pm$	240

Drell–Yan production of sleptons have smaller cross–sections which nevertheless result in observable numbers of events. It is therefore possible to to study the jet–less signatures induced by these processes.

4 Studies of exclusive signatures

4.1 Search for the $h \to \bar{b}b$ decay

The cascade decay:

$$\begin{array}{rcl} \tilde{q}_L & \to & \tilde{\chi}_2^0\, q \\ & & \hookrightarrow h\, \tilde{\chi}_1^0 \end{array} \qquad (1)$$

has a branching fraction of 23 %, which means that at least one h is produced in roughly 30 % of the SUSY events. Exploiting the b–tagging capabilities of the ATLAS detector, the h can be searched for in the dominant $h \to \bar{b}b$ decay channel. The signature is a $\bar{b}b$ pair with invariant mass peaking around the h mass, E_T^{miss} and high p_T jets.

The following selection cuts against SM and SUSY combinatorial background were applied:

- E_T^{miss}> 300 GeV;
- 2 tagged b-jets with $p_T^{b-jet} > 50$ GeV;

- veto on 3^{rd} b-jet with $p_T^{b-jet} > 15$ GeV;
- At least 2 jets with $p_T^{jet} > 100$ GeV;
- veto isolated leptons with $p_T^{lep} > 10$ GeV.

The two first requirements alone are enough to give a clear $h \to \bar{b}b$ signal peak over the combinatorial background from SUSY and over the SM background, as can be seen in the top part of Fig. 2.

The other cuts are meant to enhance the purity of the $h \to \bar{b}b$ sample which can then be used for more detailed studies on the structure of the SUSY signal events. In particular, the requirement of additional jets is effective against the $Z \to \nu\nu$ and $W \to \tau\nu$ backgrounds and adds a safety factor against badly measured multijets events where 2 jets are misidentified as b–jets.

Table 4: *Expected rates for events containing a pair of b–jets with* $m_{bb} = m_h \pm 25$ *GeV for an integrated luminosity of* $3 \cdot 10^4$ pb^{-1}

Process	Cuts 1 and 2	All cuts
SUSY all	3790	2560
SUSY $h \to \bar{b}b$	2520	1940
$\bar{t}t$	135	40
W + jets	50	5
Z + jets	130	31

The m_{bb} spectra for the signal and the background after all cuts are shown in the bottom part of Fig. 2.

A fit of the peak, after appropriate calibration of the energy of the bi–jets [12], allows to perform a measurement of the h mass with an error of the order of 1 GeV, dominated by the expected 1% uncertainty on the hadronic energy scale of the ATLAS calorimeters.

4.2 Search for $\tilde{q}_L$ in $\tilde{q}_L \to qh\tilde{\chi}_1^0$

The pure sample of $\tilde{q}_L \to q\tilde{\chi}_2^0$ decays selected as described in the previous section can be used to try to extract information on the mass of $\tilde{q}_L$. If the jet from the $\tilde{q}_L$ decay can be identified, the distribution of its invariant mass with the reconstructed $h \to \bar{b}b$ should exhibit a shape sensitive to the value of $m_{\tilde{q}_L}$.
A particularly clean event topology would arise from the associated production

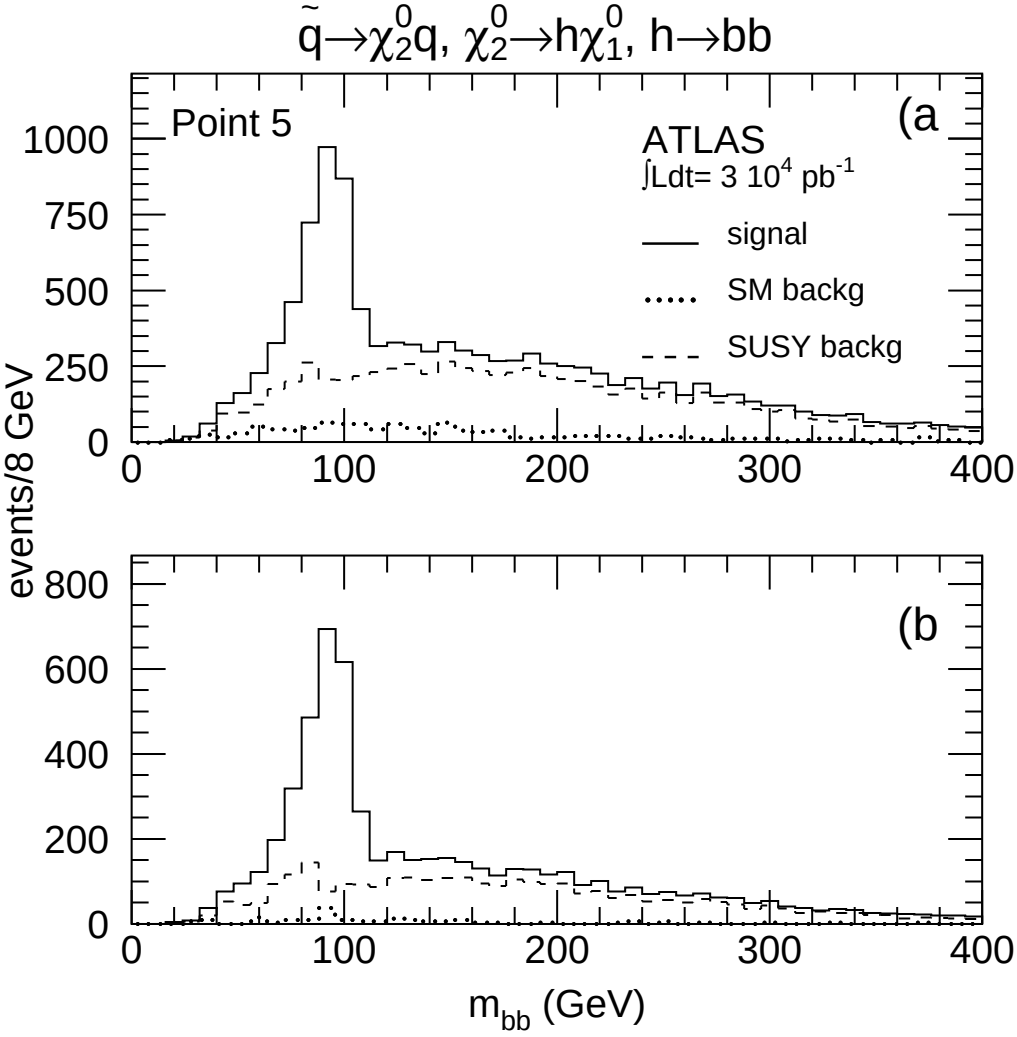

Figure 2: *For an integrated luminosity of* $3 \cdot 10^4$ pb^{-1} *distributions of the invariant mass of pairs of reconstructed b–jets for the SM background alone (dotted), the total SM + SUSY background (dashed), and the summed signal and background events (full histogram). The results are shown for events with* $E_T^{miss} > 300$ GeV *and two tagged b–jets (top) and for events passing all cuts (bottom).*

$\tilde{q}_L\tilde{q}_R$, which has a final state signature containing 2 jets + h + E_T^{miss}.
As shown in Table 5, the selected events are dominated by $\tilde{g}\tilde{q}$, which has a much

Table 5: *Expected rates of events containing a $\bar{b}b$ pair with $m_{bb} = m_h \pm 25$ GeV after selection cuts (see text) as a function of the E_T threshold applied to veto additional jets*

	No Veto	100 GeV	75 GeV	50 GeV	30 GeV
Total	2550	1390	980	565	315
$\tilde{q}_L\tilde{q}_R$	565	445	400	325	218
$\tilde{q}\tilde{g}$	1260	580	340	130	35
$\tilde{q}_L\tilde{q}_L$	340	170	110	62	9
$\tilde{g}\tilde{g}$	280	120	70	14	5

more complicated final state topology, and $\tilde{q}_L\tilde{q}_R$ production only accounts for $\approx 20\%$ of the events. However, given the mass difference between gluinos and squarks ($\approx$80 GeV), the additional jets from the decay $\tilde{g} \to q\tilde{q}$ are softer than the jets from $\tilde{q}_L \to q\tilde{\chi}_2^0$ decays. Therefore, in most cases, the jet produced in the $\tilde{q}_L \to q\tilde{\chi}_2^0$ decay is one of the two hardest jets.
Fig. 3 shows the invariant mass m_{bbj} for the events with m_{bb} inside a $\pm$25 GeV mass window around the Higgs mass peak, where the jet j is the highest or the second highest p_T jet in the event, or the one giving the minimum m_{bbj}. In the latter two cases an edge–like structure is visible, with a tail towards high masses which makes the precise measurement of the edge position difficult.

The fraction of $\tilde{q}_L\tilde{q}_R$ events can be enhanced by vetoing additional high p_T jets, but, given the softness of the additional jets, a severe veto must be applied in order to obtain a reasonable purity. The composition of the sample is shown in Table 5 for the original sample and for samples for which a third jet with a p_T greater than the cut value is vetoed.

Fig. 4 shows the minimum m_{bbj} invariant mass distribution with a jet veto set at 75 GeV. The expected rate is $\approx$ 950 events for an integrated luminosity of $3 \cdot 10^4$ pb^{-1} and the tail towards high values is substantially reduced. The invariant mass spectrum is sensitive to the $\tilde{q}_L$ mass, as can be observed in Figs. 5 and 6, where the spectrum is shown for three different values of the $\tilde{q}_L$ mass, both with and without jet veto.

From these plots, a statistical uncertainty on $\tilde{q}_L$ mass measurement of $\pm$10 GeV can be estimated for an integrated luminosity of $3 \cdot 10^4$ pb^{-1}.
The main instrumental uncertainty is the 1 % uncertainty on the jet energy scale, contributing an error of $\pm$7 GeV to the measurement.
Strictly speaking, the edge measurement should not be directly translated into

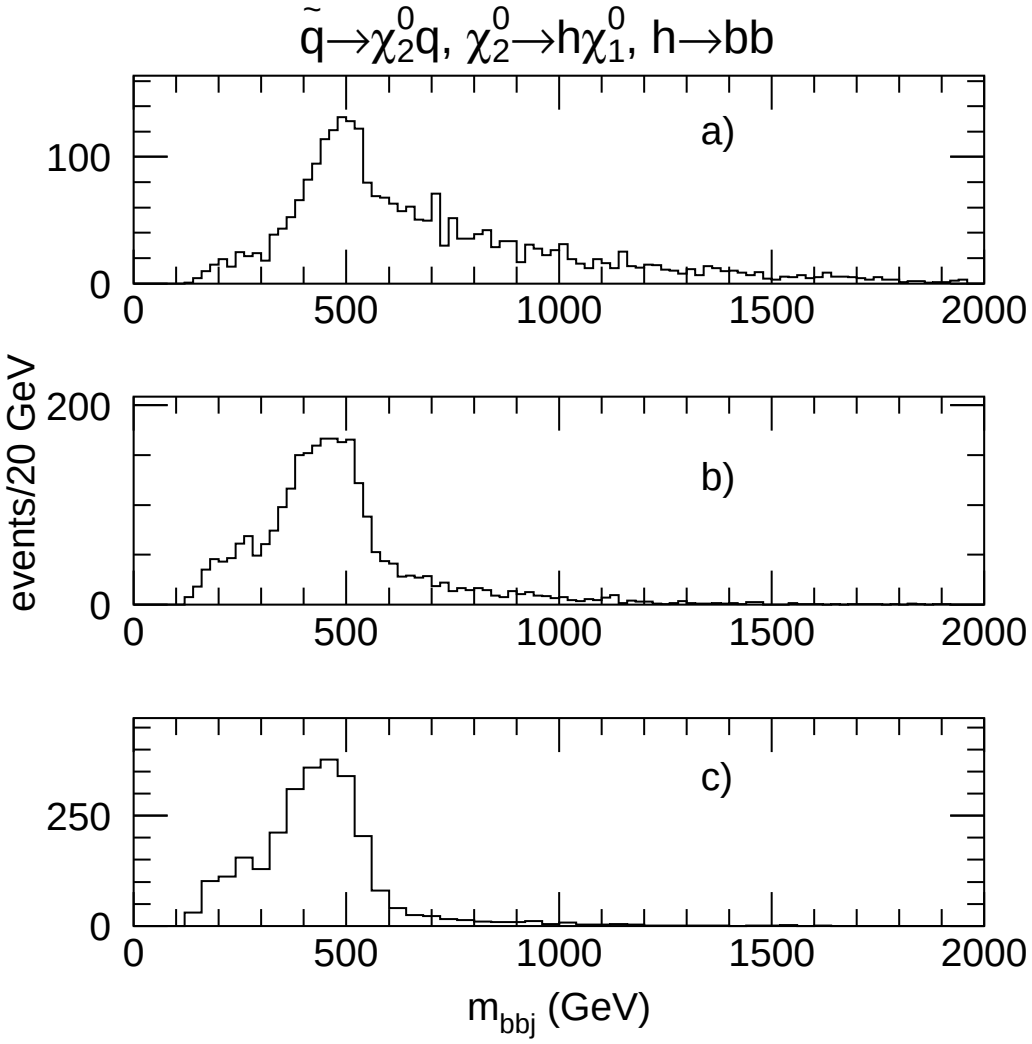

Figure 3: *For an integrated luminosity of* $3 \cdot 10^4$ pb^{-1} *distribution of the invariant mass* m_{bbj}*, where the jet* j *is: a) the hardest jet in the event; b) the second hardest jet in the event; c) the jet for which* m_{jjb} *is minimum*

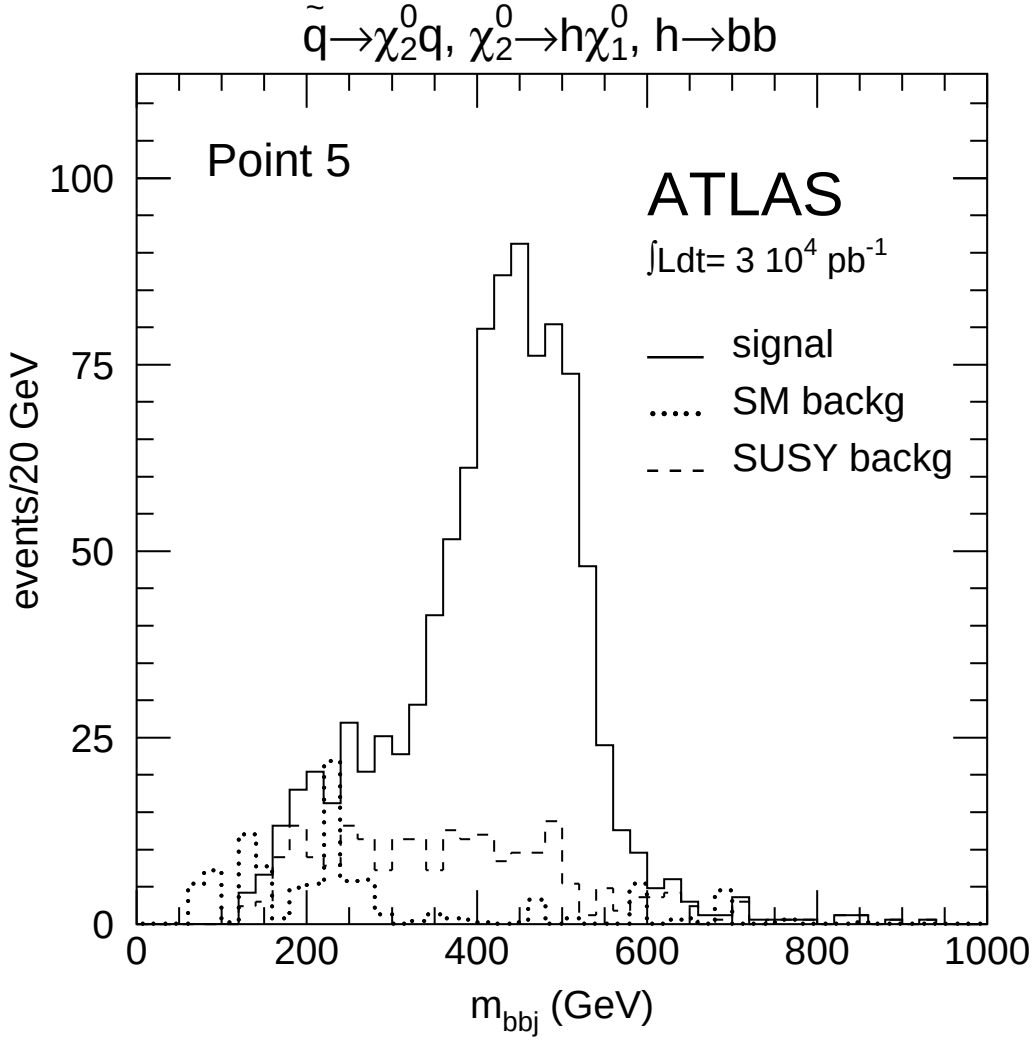

Figure 4: *For an integrated luminosity of* $3 \cdot 10^4$ pb^{-1} *distribution of the minimum* m_{bjj} *for events passing selection cuts, and after applying a jet veto at 75 GeV. The distributions are shown for the SM background (dotted), SUSY background (dashed), and signal + SUSY background (full line).*

an uncertainty on the value of the $\tilde{q}_L$ mass. In fact, the edge position depends as well on the values of $m_{\tilde{\chi}_2^0}$ and $m_{\tilde{\chi}_1^0}$. However, for this point, one can expect very precise constraints on neutralino masses from different final state signatures involving leptons, and the final constraints on the masses will result from the combined consideration of all studied signatures.
In view of these considerations, the total uncertainty on the $\tilde{q}_L$ from this measurement is expected to be ± 12 GeV for an integrated luminosity of $3 \cdot 10^4\ pb^{-1}$. For a tenfold increase in luminosity, the total error will be dominated by the energy scale error, yielding an uncertainty of ± 7 GeV for an integrated luminosity of $3 \cdot 10^5\ pb^{-1}$.

4.3 Search for $\tilde{q}_R$ in $\tilde{q}_L\tilde{q}_R$ production

The events used to measure the $\tilde{q}_L$ mass can also be used to extract information on the $\tilde{q}_R$ mass. By looking at Table 5, one can observe that after applying a hard jet veto the selected sample is dominated by $\tilde{q}_L\tilde{q}_R$ production. One of the two leading jets has been used to obtain the m_{bbj} minimum invariant mass, which was used in the previous section to extract a measurement of the $\tilde{q}_L$ mass, and therefore identified as coming from the $\tilde{q}_L$ decays. The second high-p_T jet can then be assigned to the decay $\tilde{q}_R \to q\tilde{\chi}_1^0$, and its p_T distribution can be studied to extract information on the $\tilde{q}_R$ mass.

Unfortunately, the statistical power of the sample is greatly impaired by the reduction in available number of events due to the low signal efficiency of the jet veto cut (see Table 5). Following the argument in the previous section, however, even by releasing the jet veto value, the sensitivity to the $\tilde{q}_R$ mass is retained. Most of the events which feed into the sample arise in fact from $\tilde{q}_L\tilde{g}$ production, of which $\approx 30\%$ still includes a $\tilde{q}_L\tilde{q}_R$ final state, and even in this case, the jet from $\tilde{q}_R$ decay is one of the two highest–p_T jets.

If the jet veto value is released, the additional problem arises that with a less pure sample, the p_T distribution of the second jet becomes sensitive to the $\tilde{q}_L$ mass as well, and it becomes difficult to disentangle the two contributions.
With these caveats, the optimum sensitivity is obtained for a jet veto value of 50 GeV. From the Kolmogorov test on the plots shown in Fig. 7, a sensitivity to $\tilde{q}_R$ mass of ± 50 GeV for an integrated luminosity of $3 \cdot 10^4\ pb^{-1}$ was estimated, as usual, assuming that the mass of the $\tilde{\chi}_1^0$ is known. For an integrated luminosity of $3 \cdot 10^5\ pb^{-1}$ the sensitivity will be around ± 15 GeV, still dominated by the statistical error.

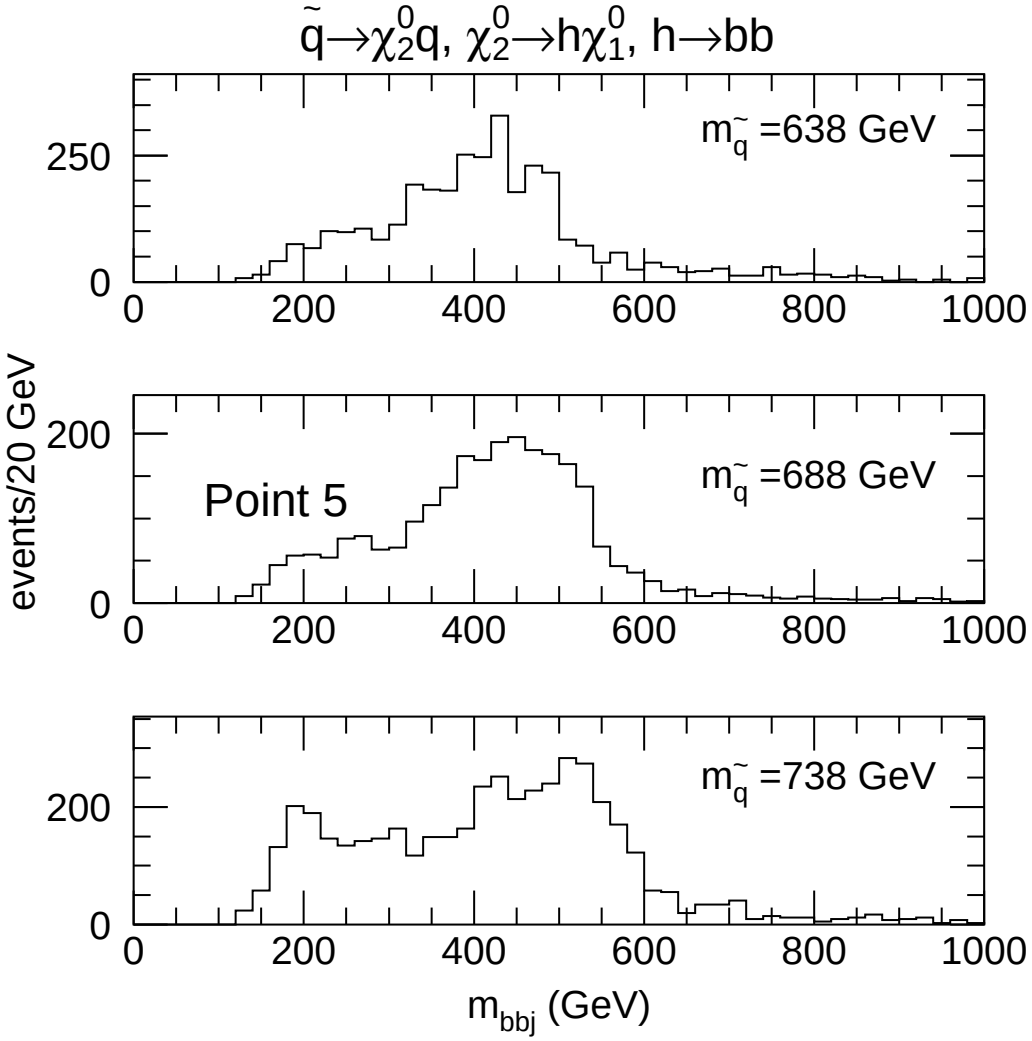

Figure 5: *For an integrated luminosity of* $3 \cdot 10^4\ pb^{-1}$ *distributions of the* m_{jbb} *minimum invariant mass for all events passing the selection cuts except the jet veto, for three different values of* q_L *mass:* $m_{q_L} = 638\ GeV$ *(top),* $m_{q_L} = 688\ GeV$ *(middle)* $m_{q_L} = 738\ GeV$ *(bottom).*

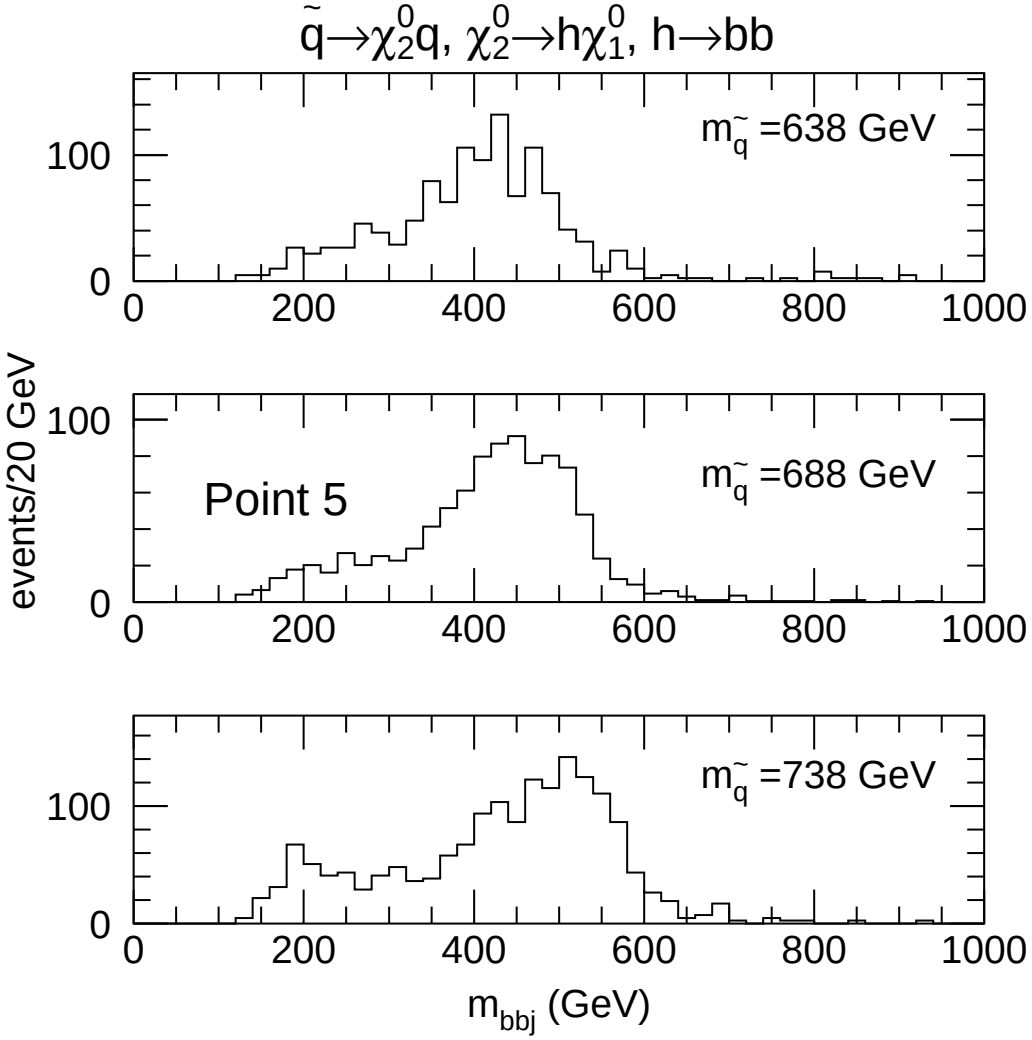

Figure 6: *The same as Fig. 5 for events passing in addition a jet veto cut at 75 GeV*

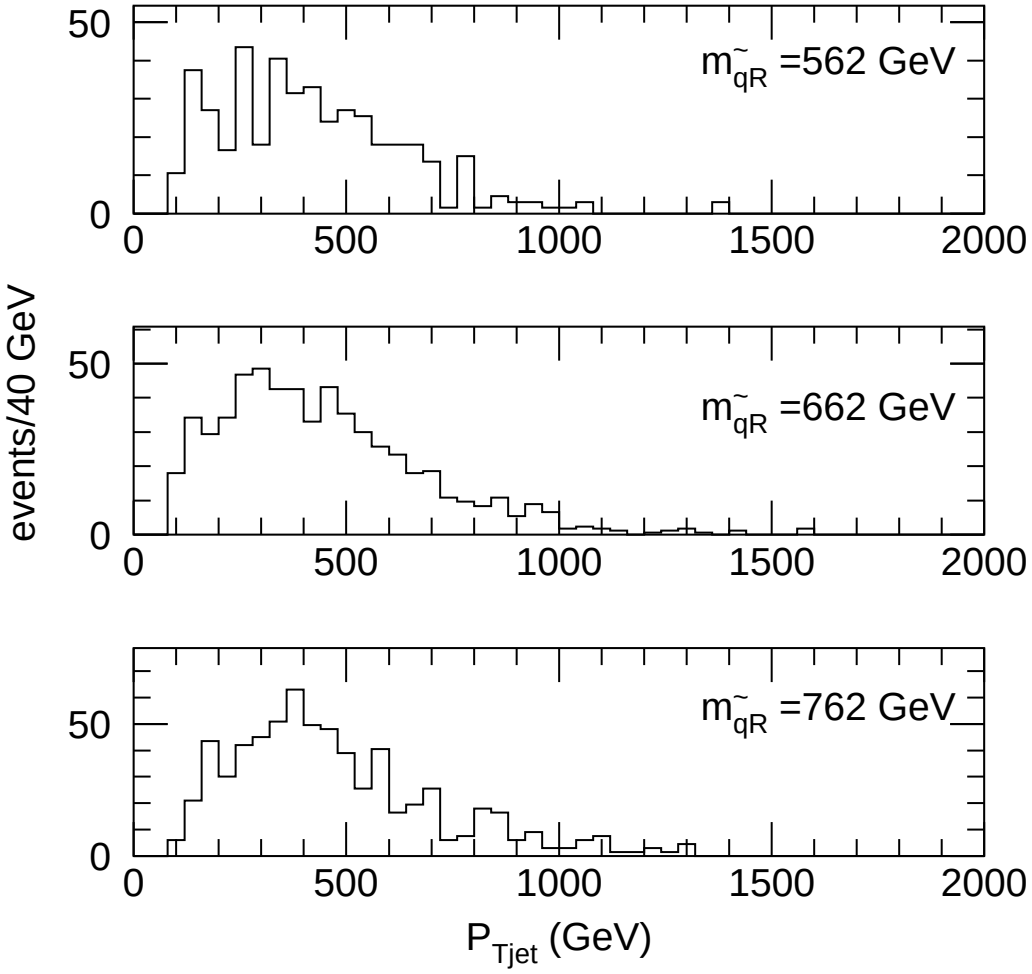

Figure 7: *For events passing the $h \to bb$ selection cuts + a jet veto cut at 50 GeV, Pt distribution of the second jet for three different values of the $\tilde{q}_R$ mass: $m_{q_R} = 562$ GeV (top), $m_{q_L} = 662$ GeV (middle) $m_{q_L} = 762$ GeV (bottom).*

4.4 Search for sleptons in 2–leptons + jets events.

As shown in 2, the second lighter neutralino $\tilde{\chi}_2^0$ also has a substantial branching fraction into sleptons. The cascade decay:

$$\begin{array}{rcl} \tilde{\chi}_2^0 & \rightarrow & \tilde{\ell}_R l \\ & & \hookrightarrow \tilde{\chi}_1^0 l \end{array} \tag{2}$$

with l = e or μ, has a branching fraction of 17%, and produces events with two high–p_T opposite–sign, same–flavour leptons, large E_T^{miss} and high p_T–jets.

Events were selected by requiring:

- E_T^{miss}> 300 GeV
- two same–flavour, opposite–sign leptons with $p_T^{lep} > 10$ GeV (a veto on additional leptons was also applied)
- at least two jets with $p_T^{jet} > 150$ GeV

The IVB + jet background is suppressed by the requirement of two high–p_T jets, and the $\bar{t}t$ background is suppressed by the hard kinematics.

For an integrated luminosity of $3 \cdot 10^4$ pb^{-1} the expected rate after selection is: 5800 signal, 880 SUSY background 120 SM background events. The sample thus obtained is very pure, and the remaining SUSY background can be subtracted by using opposite–flavour lepton pairs.

The invariant mass of the two leptons presents a very sharp edge, as shown in Fig. 8. The presence of the edge is not in itself a guarantee of the observation of the sleptons. In fact, it could be produced either by the direct $\tilde{\chi}_2^0 \rightarrow \tilde{\chi}_1^0 l^+ l^-$ three-body decay, or by the two–body decay into sleptons. The slepton signal in these events is demonstrated by the rate of the observed two–lepton signal, which is of the same order of magnitude of the $\bar{b}b$ signal coming from the two–body decay $\tilde{\chi}_2^0 \rightarrow \tilde{\chi}_1^0 h$ studied in section 4.1. A three–body decay is kinematically strongly suppressed with respect to a two–body decay, and would have a much smaller rate. Therefore these events must come from a competing 2–body decay, and the only kinematically open possibility is the decay chain through the sleptons.

The position of the edge can be measured with a precision of ≈ 0.5 GeV and

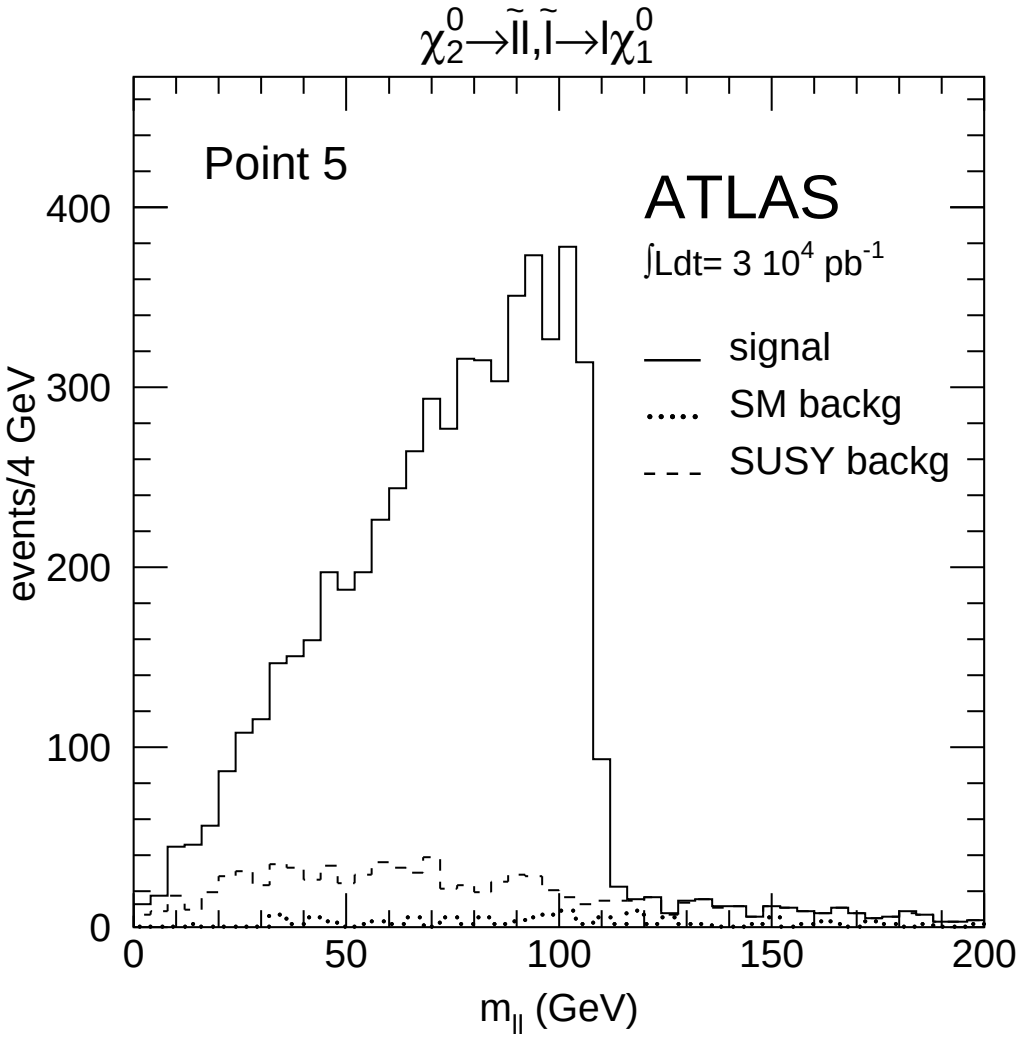

Figure 8: *For an integrated luminosity of* $3 \cdot 10^4$ pb^{-1} *two–lepton invariant mass distribution for events passing selection cuts (see text). The distribution is shown for SM background (dots), SUSY background (dashed), and summed signal and background (full line).*

is a function of the masses of the involved particles according to the expression:

$$m_{l^+l^-}^{max} = m_{\tilde{\chi}_2^0} \sqrt{1 + \frac{m_{\tilde{\ell}_R}^2}{m_{\tilde{\chi}_2^0}^2}} \sqrt{1 + \frac{m_{\tilde{\chi}_1^0}^2}{m_{\tilde{\ell}_R}^2}}.$$

If the masses of $\tilde{\chi}_2^0$ and $\tilde{\chi}_1^0$ are known, the measurement of the edge position gives the mass of the right–handed slepton with a precision of ≈ 2 GeV for an integrated luminosity of $3 \cdot 10^4$ pb^{-1}.

In order to disentangle the contributions of the different masses, other variables involving the kinematics of the two leptons can be studied. In particular, the ratio of the transverse momenta of the two leptons is also very sensitive to the slepton mass. In Fig. 9 the distribution of this ratio is shown for three different values of the slepton mass.

4.5 Direct slepton search

The direct production of charged sleptons through the Drell-Yan process will result, for an integrated luminosity of $3 \cdot 10^4 pb^{-1}$, in ≈ 1200 events for $\tilde{\ell}_R$ and ≈ 600 events for $\tilde{\ell}_L$ ($l = e$ or μ).
Charged leptons in point 5 decay with 100% BR into the corresponding lepton + LSP. The final state signature is therefore 2 high p_T leptons, E_T^{miss}, and no jet activity.

The Standard Model backgrounds are: WWi production with both W–bosons decaying to the same lepton flavour , and $\bar{t}t$ where both b–jets go undetected.

The cuts applied in the analysis are:

- E_T^{miss}> 120 GeV;
- two same flavour, opposite sign leptons with $p_T^{lep} > 30$ GeV;
- Angular separation of the two leptons in the transverse plane: $\Delta\phi < 2$;
- Veto jets with p_T> 15 GeV within $|\eta| < 5$;

The strict veto cut on the jets is necessary to reduce the $\bar{t}t$ background to an acceptable level, and the lepton separation cut helps against the WW background. The quite hard cuts necessary to bring the background below the signal have as an important side–effect the almost complete disappearance of the $\tilde{\ell}_R\tilde{\ell}_R$ signal,

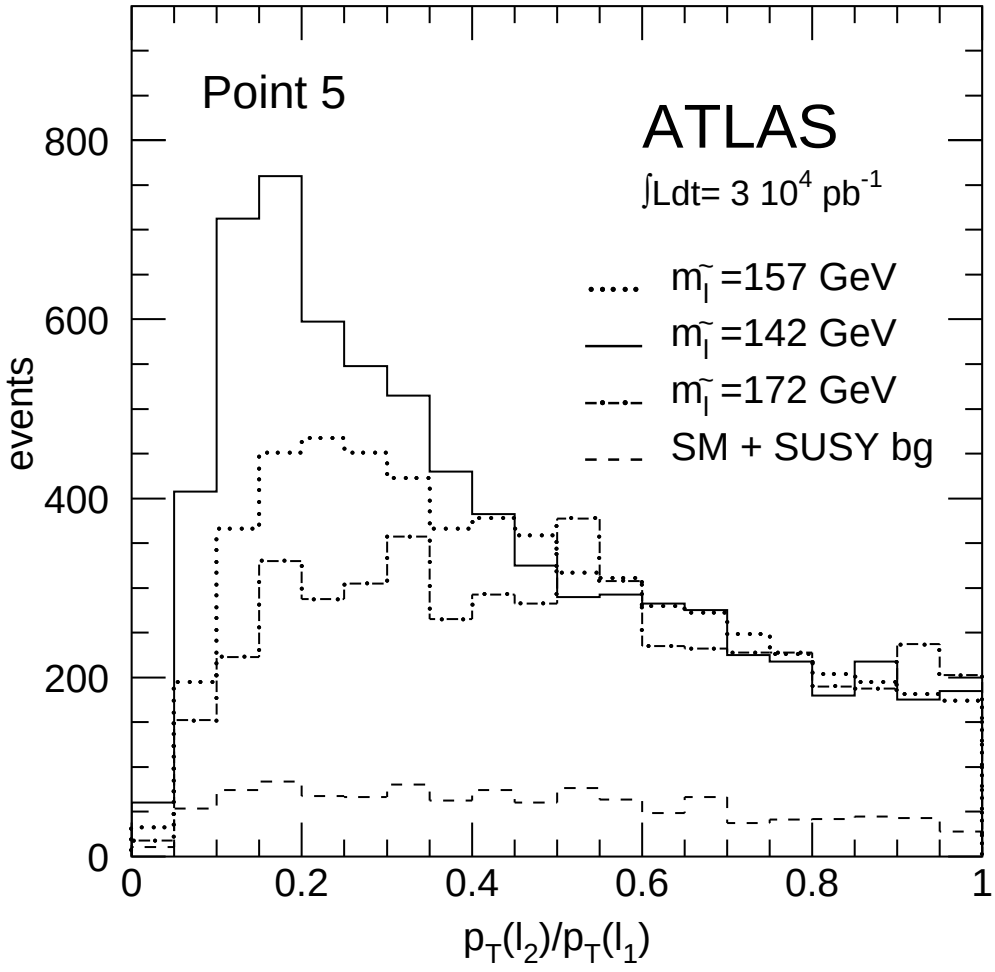

Figure 9: *For an integrated luminosity of* $3 \cdot 10^4\ pb^{-1}$ *ratio of the transverse momenta of the two leptons for three different values of the right–handed slepton mass.*

which have softer kinematics, leaving only $\tilde{\ell}_L\tilde{\ell}_L$ events in the sample. It has also been checked that the SUSY background is negligible after cuts.

This very severe jet veto cut cannot be applied at high luminosity, for which the third and fourth cuts above are substituted by:

- Angular separation of the two leptons in the transverse plane: $\Delta\phi\ < 2.5$;
- Veto jets with p_T> 40 GeV within $|\eta| < 5$;

The expected rate of signal and background for two lepton flavours are summarised in Table 6

Table 6: *Expected dilepton + E_T^{miss} rates for point 5 after cuts (see text).*

Process	$3 \cdot 10^4\ pb^{-1}$	$3 \cdot 10^5\ pb^{-1}$
$\tilde{\ell}_L\tilde{\ell}_L$	58	600
WW	14.4	140
$\bar{t}t$	4	140

With an integrated luminosity of $3 \cdot 10^5\ pb^{-1}$ direct production of left–handed sleptons can be clearly observed by ATLAS.

It is interesting to evaluate the sensitivity of the kinematical variables of the selected events to the slepton mass. As remarked above, this analysis selects the heavier slepton helicity, thus providing an information which is complementary to the one extracted by the slepton search in squark decays. Fig.10 shows the distribution of the p_T of the lepton pair, for two different values of the $\tilde{\ell}_L$ mass. From this distribution, a statistical sensitivity to the quantity $m_{\tilde{\ell}_L} - m_{\tilde{\chi}_2^0}$ of ± 10 GeV can be estimated, for an integrated luminosity of $3 \cdot 10^5\ pb^{-1}$.

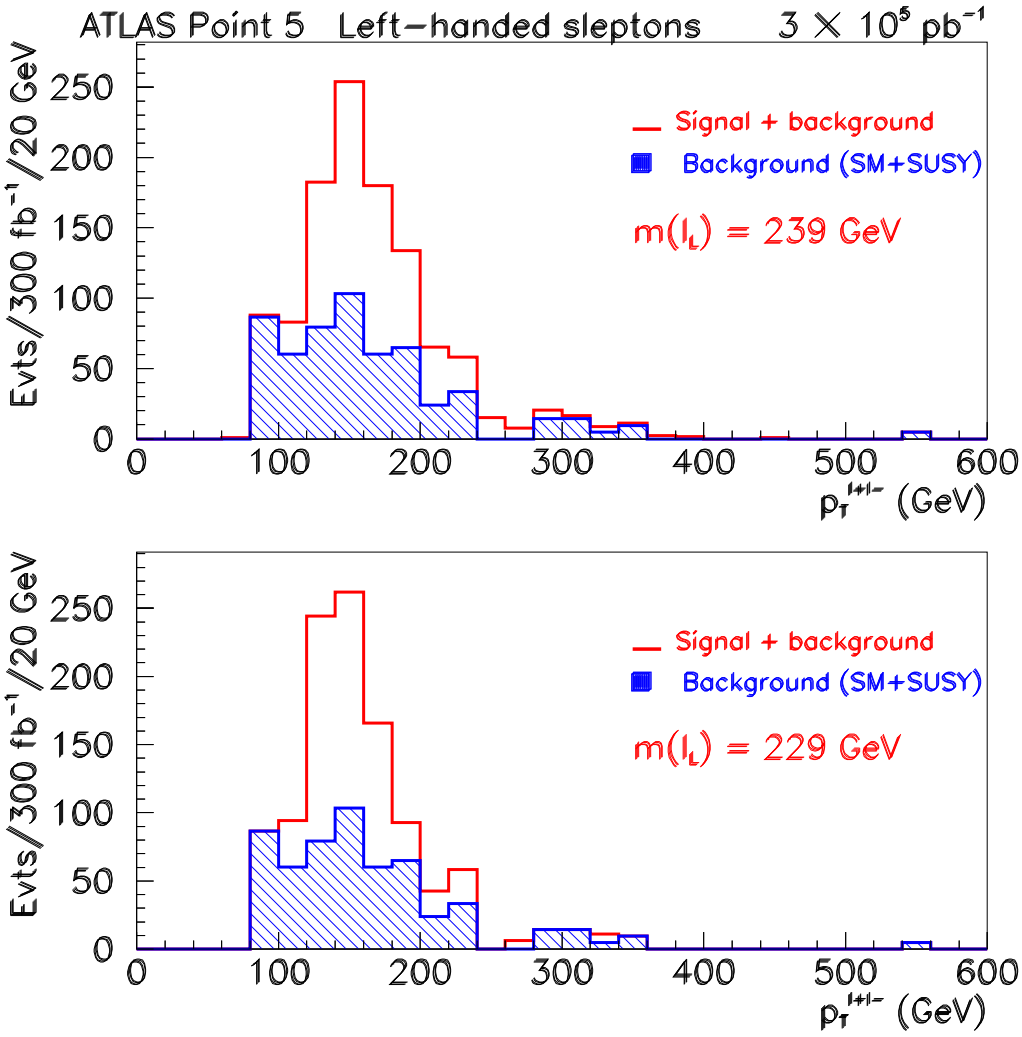

Figure 10: *Distribution of the p_T of the selected lepton pair for two values of the left–handed slepton mass.*

4.6 Search for $t\bar{t}$ pairs in SUSY events

The observation of a clean excess of $t\bar{t}$ pairs above the SM background in a sample of SUSY events can be considered as a first step in the study of $\tilde{t}_1$ decays and also of $\tilde{g} \to \tilde{t}_1 t$ decays. In fact, several cascade decay chains lead to such an excess of $t\bar{t}$ pairs:

- $\tilde{g} \to \tilde{t}_1 t \to t\bar{t}\chi_1^0$
- $\tilde{g} \to \tilde{t}_1 t \to t\bar{t}\chi_2^0$
- $\tilde{t}_1\tilde{t}_1 \to t\bar{t}\chi_1^0\chi_1^0$
- $\tilde{g}\tilde{g} \to \tilde{b}_L b\tilde{t}_1 t \to \chi_1^{\pm} t b \chi_1^{\pm} b t$

4.6.1 Extraction of $t\bar{t}$ signal in SUSY events

To select as large as possible a sample of $t\bar{t}$ pairs in the SUSY sample for point 5, a pair of hadronically decaying top quarks, accompanied by large E_T^{miss} was required using the following procedure:

1) Initial selection criteria were applied to reject as much as possible of the SM $t\bar{t}$ background:

- $E_T^{miss} > 200$ GeV;
- a lepton veto and a τ-veto;
- two tagged b-jets with $p_T^{b-jet} > 30$ GeV;
- no additional b-jet with $p_T^{b-jet} > 30$ GeV;
- at least four additional central jets ($p_T^{jet} > 30$ GeV, $|\eta^{jet}| < 3.0$).

2) A reconstruction algorithm was then applied to the selected events:

- all possible jj combinations (excluding those containing one or two tagged b-jets) are examined. All jj combinations such that $m_{jj} = m_W \pm 15$ GeV are retained. The side-bands around m_W are also considered to estimate the combinatorial background;

- for each accepted jj combination, consider each of the two possible jjb combinations (Fig. 11, top-left plot);

- choose pairs of $jjbi$ combinations such that each jet j and each tagged b is used only once in the pair (Fig. 11, top-right plot)

• for a given pair of jjb combinations compute

$\chi^2 = (m^1_{jjb} - m_t)^2 + (m^2_{jjb} - m_t)^2$;

• select the pair of jjb combinations which minimises the above χ^2 (Fig. 11, bottom-left plot);

• for the jji combinations chosen, rescale their 4–momenta to impose the constraint $m_{jj} = m_W$ (Fig. 11, bottom-right plot);

• finally, compute m_{jjb} for each of the top-quark candidates.

Fig. 11 shows the reconstructed m_{jjb} peaks described above for $\tilde{q}_R\tilde{g}$ production. In gray is shown the background obtained by plotting the m_{jjb} combinations built using jj combinations in the sidebands of the W peak. In all cases a clear excess around the top mass is observed, and the cleanest $\bar{t}t$ signal is obtained after all selection cuts.

If both jjb combinations satisfy the cut $m_{jjb} = m_{top} \pm 30\ GeV$, the event is accepted for further analysis. Table 7 shows the efficiency of this reconstruction procedure for various SUSY processes and for the SM $t\bar{t}$ background, starting from the selection cuts described above. The lowest efficiencies are observed for the SUSY processes not containing any top quark in the cascade decay chain and for the SM $t\bar{t}$ background. This is not surprising since none of the SM $t\bar{t}$ pairs selected by the above cuts can correspond to a pair of purely hadronic top-quark decays, due to the very large E_T^{miss} required in the event. Most of the remaining SM $t\bar{t}$ events were found to be $W \to \tau\nu$ decays with additional jets faking the top–quark reconstruction. After applying a τ-lepton veto, only 25% of these $W \to \tau\nu$ decays from $t\bar{t}$ production are retained.

One should also note that the overall efficiency of the kinematic reconstruction of a top-quark pair is only 3–5%, due to the complexity of the final state and to the large combinatorial background which is present for the signal events at point 5. For normal $t\bar{t}$ events, with few extra jets, this reconstruction efficiency was checked and found to be much higher.

The resulting invariant mass distributions, m_{jjb}, for after all reconstruction steps discussed above are shown in Fig. 12. The peak position is well centred around m_{top} and the side-bands (grey area), corresponding to $m_{jj} = 50 \pm 15$ GeV and $m_{jj} = 110 \pm 15$ GeV, reproduce quite accurately the shape and magnitude of the SUSY combinatorial background to the SUSY $t\bar{t}$ signal.

Fig. 13 shows the jjb invariant-mass peak after background subtraction both for the SUSY events and the small amount of residual SM background. For an integrated luminosity of $3 \cdot 10^4\ pb^{-1}$, approximately 1200 SUSY events with a

Table 7: *Reconstruction efficiencies for $t\bar{t}$ pairs from various processes for events passing the selection cuts described in the text.*

Process	Two $W \to jj$ decays	Two $t \to jjb$ decays
SUSY : $\tilde{q}_R\tilde{g}, \tilde{g} \to \tilde{t}_1 t$	29%	15%
SUSY : $\tilde{t}_1\tilde{t}_1$	29%	17%
SUSY : $\tilde{g} \to \tilde{t}_1 t$, other	36%	15%
SUSY : other	14%	5%
$t\bar{t}$	14%	6%

reconstructed $t\bar{t}$ pair ($m_{jjb} = (175 \pm 30)$ GeV for both jjb combinations) are expected above about 130 events from the SM $t\bar{t}$ background.

This sample of reconstructed top-quark pairs can then be used to:

- partially reconstruct $\tilde{g} \to \tilde{t}_1 t$ decays to estimate $m_{\tilde{g}}$;
- select $\tilde{t}_1\tilde{t}_1$ production to estimate $m_{\tilde{t}_1}$.

It should not be forgotten that the rates quoted above correspond to the more optimistic SPYTHIA values for the $\tilde{t}_1$ decay branching ratios and would be reduced if ISAJET were to be used instead.

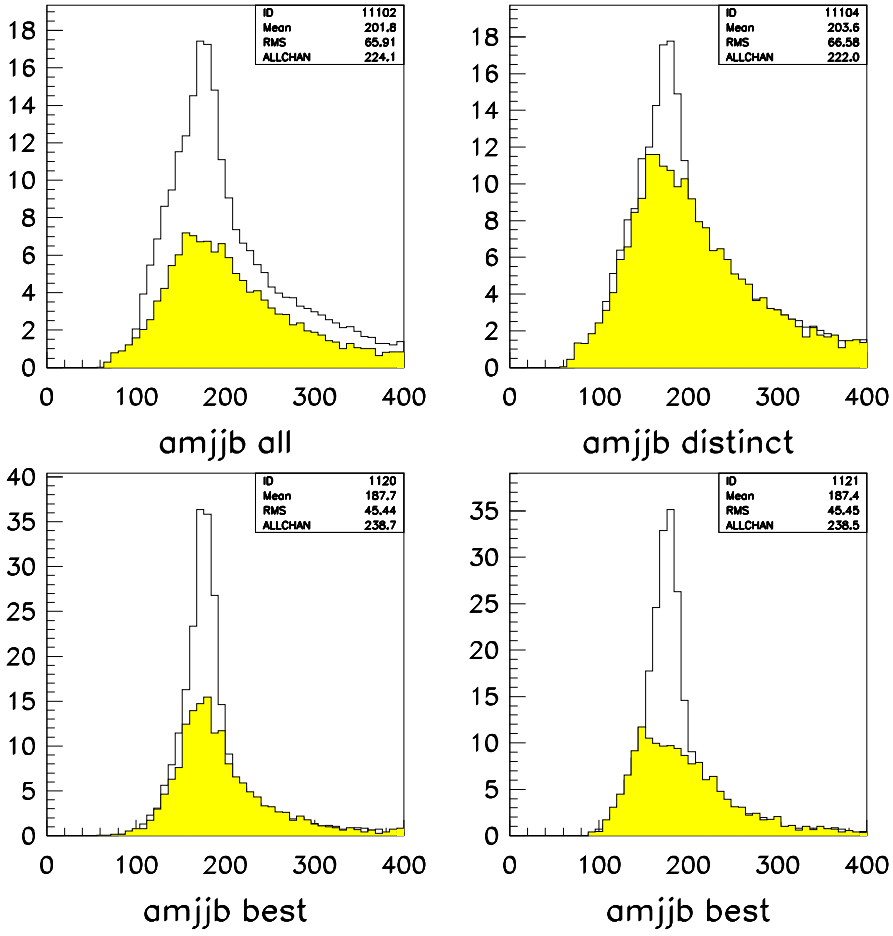

Figure 11: *For an integrated luminosity of* $3 \cdot 10^4\ pb^{-1}$ *and* $\tilde{q}_R\tilde{g}$ *production, reconstructed distribution of* m_{jjb} *peak for SUSY events passing the selection cuts described in text: all jjb combinations (top-left), only distinct jjb combinations (top-right), two best jjbi combinations without (bottom-right) and with (bottom-left)* m_{jj} *constrained to* m_W*. The shaded regions represents the SUSY combinatorial background using the side-bands around* m_W *as described in the text.*

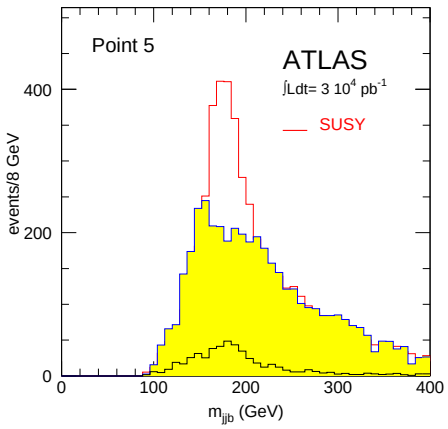

Figure 12: *For an integrated luminosity of* $3 \cdot 10^4$ pb^{-1}*, reconstructed distribution of* m_{jjb} *for SUSY events passing the selection cuts described in the text after using the constraint* $m_{jj} = m_W$ *(solid line). The light shaded area represents the SUSY combinatorial background estimated using the side-bands around* m_W*. The lowest line on shaded area shows the residual SM* $t\bar{t}$ *background.*

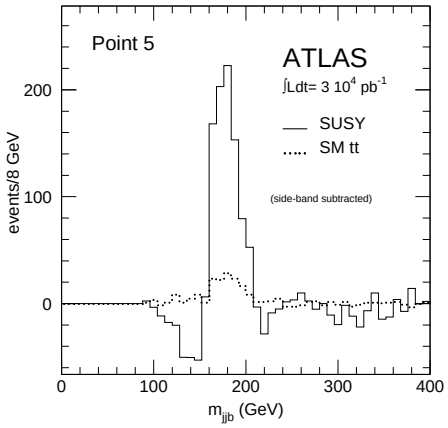

Figure 13: *Reconstructed distributions of* m_{jjb} *from Fig. 12 after subtracting the combinatorial background from SUSY events and the SM* $t\bar{t}$ *backcground events.*

4.6.2 Partial reconstruction of the $\tilde{g} \to \tilde{t}_1 t \to \tilde{\chi}_1^0 tt$ cascade

For this decay chain, the distribution of $m_{t\bar{t}}$, for events with a reconstructed pair of top quarks and large E_T^{miss} is sensitive to the gluino mass (assuming a fixed value for $m_{\chi_1^0}$) but quite insensitive to the value of the $\tilde{t}_1$ mass.

It is therefore desirable to select the $\tilde{q}_R\tilde{g}$ process, which has a production cross-section of 4.1 pb, to obtain as clean as possible a sample of $t\bar{t}$ pairs from gluino decay. In fact, all processes ($\tilde{g}\tilde{g}$, $\tilde{q}_L\tilde{g}$) which result in one $\tilde{g} \to \tilde{t}_1 t \to \chi_1^0 t\bar{t}$ cascade decay and which do not produce any other top quark, can be considered as a signal for the measurement of $m_{\tilde{g}}$. The main background to these events arises from fake top-quark pairs reconstructed in events containing b-quarks and $\chi_1^\pm \to \chi_1^0 W$ decays, as, for example, $\tilde{g} \to \tilde{b}_L b \to \chi_1^0 W t b$.

To reduce this SUSY combinatorial background, the events selected and reconstructed as described in the previous Section were required to contain at least one additional hard central jet with $p_T^{jet} > 300$ GeV and $|\eta| < 2.0$. Also, both jjb combinations were constrained to $m_{jjb} = m_{top}$. As shown in Table 8, only 480 signal events containing one $\tilde{g} \to \tilde{t}_1 t \to \chi_1^0 t\bar{t}$ cascade decay and 640 background events (predominantly from other SUSY processes) are expected after these cuts for an integrated luminosity of $3 \cdot 10^4\ pb^{-1}$. However, about 56% of the background to the signal is from squark–gluino production or gluino pair production, and the kinematical distributions for the background will display a sensitivity to $m_{\tilde{g}}$ comparable to the one observed for the signal.

Before tau-jet veto the background from $t\bar{t}$ events is from fake top reconstruction (events with $W \to \ell\nu$) and is dominated by $W \to \tau\nu$. The tau-jet veto reduces it by roughly a factor of 4.

The distribution of $m_{t\bar{t}}$ for the selected events is sensitive to $m_{\tilde{g}}$ as can be seen in Fig. 14 which shows the distributions for signal+background (solid) and signal alone (dashed) for $m_{\tilde{g}} = 697, 767, 837$ GeV and for an integrated luminosity of $3 \cdot 10^4\ pb^{-1}$. The sensitivity of the $m_{t\bar{t}}$ distributions to $m_{\tilde{g}}$ is summarised in Table 9. The gluino mass can be measured (for the top–pair events alone) to ± 20 GeV (resp. ± 11 GeV) for an integrated luminosity of $3 \cdot 10^4\ pb^{-1}$ (resp. $3 \cdot 10^5\ pb^{-1}$). This result assumes that $m_{\chi_1^0}$ is known from other constraints to an accuracy of $\sim \pm 20$ GeV.

Table 9: *Expected statistical and systematic uncertainties on the measurement of $m_{\tilde{g}}$ using events with reconstructed $t\bar{t}$ pairs and large E_T^{miss}, for integrated luminosities of $3 \cdot 10^4\ pb^{-1}$ and $3 \cdot 10^5\ pb^{-1}$*

Table 8: *Expected rates for* $\tilde{g} \to \tilde{t}_1 t$ *signal events and backgrounds, for an integrated luminosity of* $3 \cdot 10^4\ pb^{-1}$.

Process	expected rates $3 \cdot 10^4\ pb^{-1}$	expected rates $3 \cdot 10^5\ pb^{-1}$
SUSY : $\tilde{q}_R \tilde{g}, \tilde{g} \to \tilde{t}_1 t$	212	1470
SUSY : other, $\tilde{g} \to \tilde{t}_1 t$	272	1890
SUSY : $\tilde{t}_1 \tilde{t}_1$	28	190
SUSY : other,	583	4050
$t\bar{t}$	36	250

Source of uncertainties	$3 \cdot 10^4\ pb^{-1}$	$3 \cdot 10^5\ pb^{-1}$
Statistical	$\pm$ 19 GeV	$\pm$ 8 GeV
Jet energy scale ($\pm$ 1%)	$\pm$ 7 GeV	$\pm$ 7 GeV
Combined	$\pm$ 20 GeV	$\pm$ 11 GeV

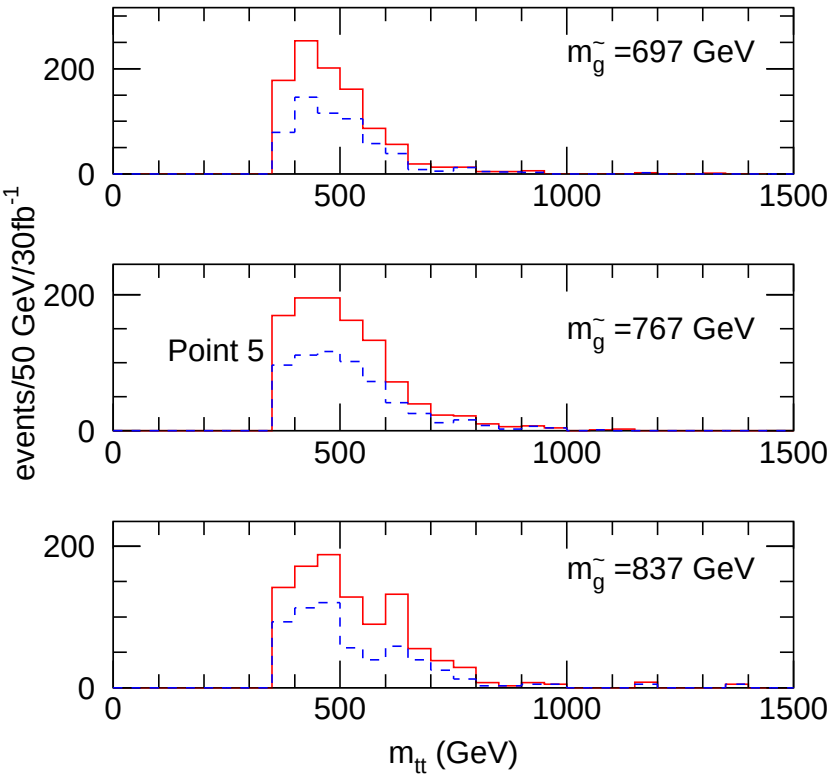

Figure 14: *Reconstructed distributions for $m_{t\bar{t}}$ for signal+background (solid histogram) and for SUSY + SM background (dashed histogram) as a function of the gluino mass, $m_{\tilde{g}}$ =697 GeV (top), 767 GeV (middle) and 837 GeV (bottom), for an integrated luminosity of $3 \cdot 10^4$ pb^{-1}.*

4.6.3 Partial reconstruction of $\tilde{t}_1\tilde{t}_1$ decays

The extraction of $\tilde{t}_1\tilde{t}_1$ pair production appears to be the only method to obtain a direct estimate of the $\tilde{t}_1$ mass. This process has a production cross-section of $\simeq$ 700 fb, and leads to $t\bar{t}\chi_1^0\chi_1^0$ final states in about 50% of the cases. After applying the selection cuts described in Section 4.6.1 to reconstruct the $t\bar{t}$ pair in the final state, less than 100 events are expected for an integrated luminosity of $3 \cdot 10^4$ pb^{-1}, with an overwhelming SUSY combinatorial background.

This channel will therefore be barely observable at low luminosity, and an integrated luminosity of $3 \cdot 10^5$ pb^{-1} will be needed in order to be able to extract information on the $\tilde{t}_1$ mass.

The very large SUSY combinatorial background can be reduced by applying tight jet veto cuts. The following additional cuts are therefore applied to the events selected by requiring a reconstructed $t\bar{t}$ pair and large E_T^{miss}:

- no jet with $p_T^{jet} > 100$ GeV and $|\eta| < 3.0$
- at most one jet with $p_T^{jet} > 50$ GeV and $|\eta| < 3.0$
- both b-jets must have $p_T^{b-jet} > 50$ GeV.

With these cuts, a signal-to-background of about 1:2 can be achieved, but with a low rate of 43 signal events above 48 events of SUSY combinatorial background and 48 background events from SM $t\bar{t}$ production, for an integrated luminosity of $3 \cdot 10^4$ pb^{-1}.

Fig. 15 shows the distributions of of p_T^{top} for the top quark with higher p_T, for three different values of the $\tilde{t}_1$ mass, and for an integrated luminosity of $3 \cdot 10^4$ pb^{-1}, both for signal+background (solid line) and for signal alone (dashed line). For an integrated luminosity of $3 \cdot 10^5$ pb^{-1} a measurement of the $\tilde{t}_1$ mass with statistical+systematic precision of $\pm$ 50 GeV can be obtained from these distributions.

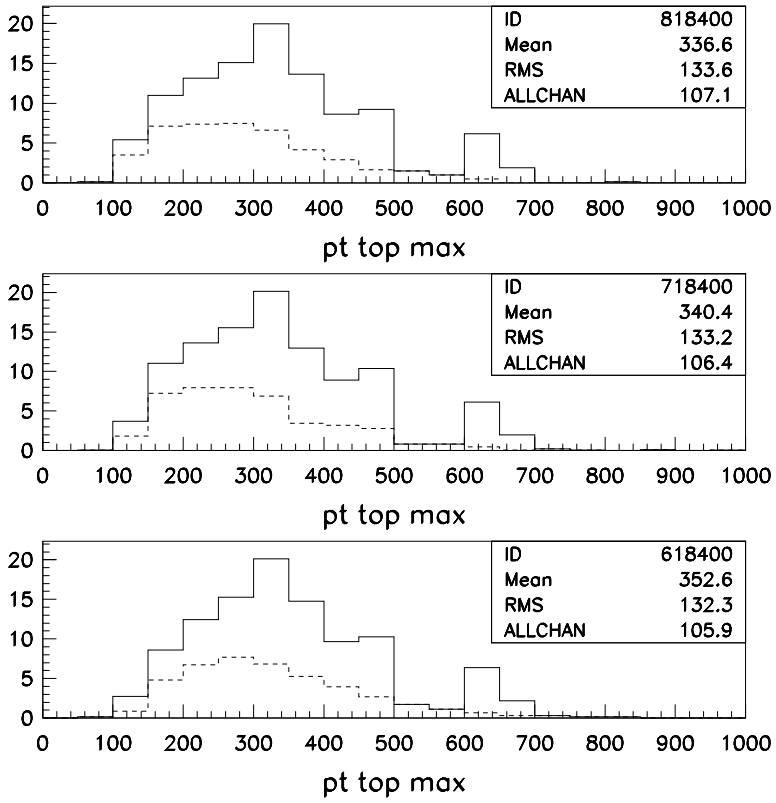

Figure 15: *Reconstructed distribution of* p_T^{top} *for the top quark with higher* p_T*, for the summed signal+background (solid histogram) and signal (hatched histogram) as a function of the* $\tilde{t}_1$ *mass, for* $m_{\tilde{t}_1}$ *= 380 GeV (top), 438 GeV (middle) and 480 GeV (bottom), for an integrated luminosity of* $3 \cdot 10^4$ pb^{-1}.

5 Constraints on tanβ and μ from the $\tilde{\chi}_2^0$ branching ratios

The branching ratios for the decays of the $\tilde{\chi}_2^0$ are a very sensitive probe of the fundamental parameters tanβ and μ. For Point 5, as shown in Section 4.1 above, a clear signal for the decay $\tilde{\chi}_2^0 \to h\tilde{\chi}_1^0$ can be observed. In Fig.16 the branching fraction for this decay is shown, as a function of tanβ and μ, with all the other SUGRA parameters fixed at their nominal values. It is clearly seen that a negative value for μ is excluded, and that the value of tanβ must be ≤ 5, in order to account for the observed signatures.

Further detailed consideration on how to exploit this kind of information in conjunction with the knowledge of the h–boson mass, can be found in [8]

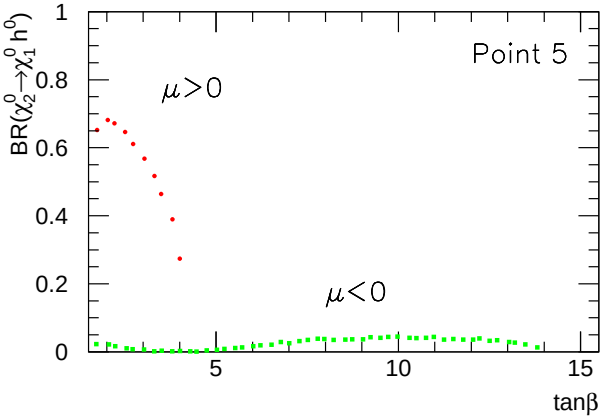

Figure 16: *Branching ratio for the decay $\tilde{\chi}_2^0 \to h\tilde{\chi}_1^0$ as a function of tanβ for the two values of the sign of μ.*

6 Conclusions

The point in SUGRA parameter space discussed in this paper yields final state signatures which are particularly favourable both in terms of supersymmetry

discovery and detailed studies of exclusive channels.

Squarks and gluino masses in the region around 600–700 GeV provide a large rate of SUSY events, and at the same time a hard E_T^{miss}spectrum which allows easy discovery in the 'classical' E_T^{miss}+ jets signature.

The 70 % branching ratio of $\tilde{\chi}_2^0$ into h$\tilde{\chi}_1^0$ provides with the reconstruction of the $\bar{b}b$ peak from $h \to \bar{b}b$ decays, a good tag for $\tilde{q}_L$ decays, allowing to measure the $\tilde{q}_L$ mass with a statistical precision of $\simeq 12$ GeV for an integrated luminosity of $3 \cdot 10^4$ pb^{-1} Using the same events it is also possible to obtain information on the $\tilde{q}_R$ mass by looking at the hardest jet not used to reconstruct the $\tilde{q}_L$ decay.

The relatively light sleptons can be observed and measured both in the decay of $\tilde{\chi}_2^0$ and in direct Drell–Yan production. A very interesting feature is the possibility to measure separately the masses of $\tilde{\ell}_L$ and $\tilde{\ell}_R$, thus providing strong support to the hypothesis that the observed signal is produced by a supersymmetric theory.

The decay chain $\tilde{g} \to \tilde{t}_1 t \to \tilde{\chi}_1^0 tt$ and $\tilde{t}_1$ direct pair production can be identified by reconstructing the hadronic decays of both top quarks. These events can be used to extract information on the masses of $\tilde{g}$ and of $\tilde{t}_1$.

The various constraints on the SUSY particle masses obtained in this way are summarised in Table 10. These measurements allow to extract the parameters of the model, and even to overconstrain it. The iterative technique used to perform this calculation is described in detail in [8], and the results are shown in Table 11.

Table 10: *Estimated accuracies of the sparticle mass measurements from the analyses discussed in the text for luminosities of* $3 \cdot 10^4$ pb^{-1} *and* $3 \cdot 10^5$ pb^{-1}

Variable	Value (GeV)	Accuracy ($3 \cdot 10^4$ pb^{-1}) (GeV)	Accuracy ($3 \cdot 10^5$ pb^{-1}) (GeV)
m_h	92.9	± 1.0	± 0.2
$m_{l^+l^-}$ edge	108.7	± 0.5	± 0.2
$m_{\tilde{\ell}_R}$	157.2	± 1.9	± 0.5
$m_{\tilde{\ell}_L}$	239	± 10	± 3
$m_{\tilde{q}_L}$	688	± 12	± 7
$m_{\tilde{q}_R}$	662	± 40	± 20
$m_{\tilde{g}}$	767	± 20	± 11
$m_{\tilde{t}_1}$	493		± 50

Table 11: *SUGRA parameter measurement accuracies for three different assumptions on the integrated luminosity (see [8])*

SUGRA parameter	Initial	High	Ultimate
m_0 = 300 GeV	±8 GeV	±4 GeV	±4GeV
$m_{1/2}$ = 100 GeV	±5 GeV	±5 GeV	±3GeV
tanβ= 2.1	±0.11	±0.08	±0.02

References

[1] ATLAS Technical Proposal, CERN/LHCC/94-43 (1994)

[2] See e.g. references in H. Baer et al.: Low Energy Supersymmetry Phenomenology, FSU-HEP-950401 (1995); see also [4] below

[3] Precision SUSY measurement with ATLAS,transparencies of the LHCC Workshop, available at:
http://Atlasinfo.cern.ch/Atlas/GROUPS/PHYSICS/SUSY/susy.html

[4] I. Hinchliffe et al. ATLAS Note PHYS-No-107

[5] E. Richter–Was et al. ATLAS Note PHYS-No-108

[6] E. Nagy et al ATLAS Note PHYS-No-109

[7] F. Gianotti ATLAS Note PHYS-No-110

[8] D. Froidevaux et al. ATLAS Note PHYS-No-112

[9] F. Paige and S. Protopopescu, in Supercollider Physics, p 41, ed. D. Soper (World Scientific, Singapore, 1986);

[10] S. Mrenna, SPYTHIA, A Supersymmetric Extension of PYTHIA 5.7; ANL-HEP-PR-96-63(1996)

[11] M Carena, M. Quiros and C.E.M. Wagner, Nucl. Phys, B461 (1996),47

[12] E. Richter–Was, D. Froidevaux, and L. Poggioli, ATLAS Internal Note PHYS-No-079

[13] J. Ellis et al. Nucl Phys. B238, 453 (1984);

[14] H. Baer, M Brhlik, Phys. Rev, D53, 597 (1996).